

# Testing of Micro-optics using Digital Holographic Interferometric Microscopy

Varun Kumar and Chandra Shakher

*Laser Applications and Holography Laboratory, Instrument Design Development Centre,  
Indian Institute of Technology Delhi, Hauz Khas, New Delhi 110016, India*

**Keywords:** Digital Holographic Interferometric Microscopy, Phase Map, Micro-lens Array, Micro-optics.

**Abstract:** Digital holographic interferometric microscopy (DHIM) is used as metrological tool for the testing of micro-optics. The paper presents the measurement of sag height ( $h$ ), radius of curvature (ROC), and shape of micro-lens. The advantage of using the DHIM is that the distortions due to aberrations in the optical system are avoided by the interferometric comparison of reconstructed phase with and without the object.

## 1 INTRODUCTION

Micro - optical component such as microlenses and micro lens array have numerous engineering and industrial applications for collimation of laser diode, imaging for sensor system (CCD/CMOS, document copier machines etc.), for making beam homogeneous for high power laser, a critical component in Shack-Hartmann sensor, fiber coupling and optical switching in communication technology (Sinzinger 1999, Anderson 1997, Cormick et al,1999, Hou et al. 2015). Also micro-optical components have become an alternative to bulk optics for applications where miniaturization, reduction of alignment and packaging cost are necessary (SUSS MicroOptics SA catalog 2007). The compliance with high-quality standards in the manufacturing of micro-optical components is a precondition to be compatible on worldwide markets. Therefore, high demands are put on quality assurance. For quality assurance of these lenses, an economical measurement technique is needed. For cost and time reason, technique should be fast, simple, and robust with high resolution. The technique should provide non contact, non-invasive and full field information about the shape of micro-optical component under test. The interferometric techniques are noncontact type, non invasive and provide full field information about the shape of the optical components. The conventional interferometric technique such as Mach-Zehnder interferometry, Twyman- Green interferometry and

white light interferometry are available for testing of micro-optics (Reichelt et al., 2005; Weible et al., 2004; Wahaba and Kries, 2009). However, interferometric techniques needs more experimental efforts for phase measurement (such as phase shifting techniques) and are thus time consuming (Reichelt et al., 2005; Weible et al., 2004; Wahaba and Kries, 2009; Zhang and Yamaguchi, 1998). White light interferometry is not suited to measure entire lens profile and yields accurate information only for vertex of micro-lens (Weible et al., 2004). Digital holography (DH) overcomes the above discussed problems. Digital holographic microscopy (DHM) allows to extract both the amplitude and phase information of a wavefront transmitted through the transparent object (micro-lenses array) from a single digitally recorded hologram by use of numerical methods (Charrière et al.,2006; Schnar and Juptner, 1994; Cuche et al. 1999; Cuche et al. 1999, p. 291-293; Schnar, 2005). Due to numerical reconstruction, the complex object wavefront at different distances can be reconstructed. Digital holography provides axial resolution in nanometers while lateral resolution is limited by diffraction and the size of the sensor (Cuche et al. 1999; Cuche et al. 1999, p. 291-293).

In this paper, Mach-Zehnder based digital holographic interferometric system (DHIM) is used for the testing of refractive micro lens. The advantage of using the DHIM is that the distortions due to aberrations in the optical system are avoided by the interferometric comparison of reconstructed phase with and without the micro lens array (Anand

et al., 2011, p. 547). In the experiment, first a digital hologram is recorded in the absence of micro-lens array which is used as a reference hologram. Second hologram is recorded in the presence of micro-lens array. The presence of transparent micro-lens array will induce a phase change in the transmitted laser light. Complex amplitude of object wavefront in presence and absence of micro-lens array is reconstructed by using Fresnel reconstruction method (Schnar and Juptner, 2005). From the reconstructed complex amplitude, one can evaluate the phase of object wave in presence and absence of micro-lens array. Phase difference between the two states of object wave will provide the information about optical path length change occurring between two states. By knowing the value of the refractive index of micro-lens array material and air, the surface profile of micro-lens array is calculated. From the experimentally calculated value of sag height ( $h$ ) and diameter of micro-lens ( $D$ ), the radius of curvature of micro-lens is calculated.

## 2 EXPERIMENTAL SET UP AND THEORY

Figure 1 shows the schematic of experimental set up of digital holographic microscope. The Experimental set up is based on Mach-Zehnder interferometer. A 5 mW He-Ne laser (Make – Melles Griot,  $\lambda=632.8$  nm) is used as a light source. Light from the laser source is divided into two beams using a beam splitter BS1. One of the beams acts as a reference beam and the other acts as an object beam. Light in the two arms of the interferometers are expanded and collimated by assembly of spatial filter (SF) [Make – Newport Corp.] and collimating lens (CL). Light in the one arm is passed through the object under test (micro-lenses array). In the experiment, round shape and plano-convex micro lens array supplied by THORLABS with micro lens sag height ( $h=0.87$   $\mu\text{m}$ ), diameter ( $D=146$   $\mu\text{m}$ ) and radius of curvature ( $\text{ROC}=3.063$  mm) was used. The object under test was mounted on 2D translation stage in the object arm of the Mach-Zehnder interferometer and a microscope objective (20 X, NA=0.40) was used to increase the lateral resolution of the digital holographic microscopic system. A similar microscope objective (20X, NA=0.40) was also used in the reference arm of the interferometer to match the curvature in the object and reference wavefront. A minute angle is introduced in the reference beam

to make the off axis holographic system. The microscope objectives in both arms and beam splitter are adjusted in such a way that the interference fringes are straight; this avoids the need to perform any digital correction due to spherical aberration introduced by microscope objectives (Anand et al., 2011, p. 547). ND filters are used in the reference arm and object arm to adjust the intensity for recording good contrast fringes in the hologram. All the optical components (mirrors, lenses, beam splitters, ND filters) used in the experiments are supplied by M/S Melles Griot (Netherland).

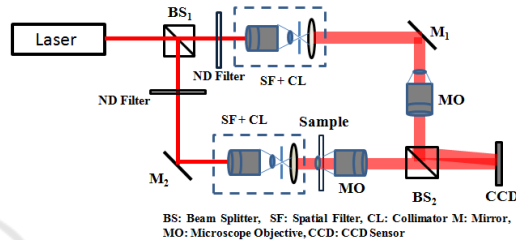


Figure 1: Mach-Zehnder interferometer based Digital Holographic Microscope for testing of micro lens array.

The object beam interferes with the reference beam at the hologram plane (CCD Plane). The hologram with intensity (Schnar and Juptner, 2005)

$$H(X, Y) = |R|^2 + |O|^2 + R^* O + RO^* \quad (1)$$

is recorded by CCD sensor (Make – Lumenera Corporation, Model – Infinity3-1M). In equation 1, R is the reference wavefront and O is the object wavefront, and \* denote the complex conjugate. The pixel size on CCD sensor is  $6.45\mu\text{m} \times 6.45\mu\text{m}$ . Total numbers of pixels are  $1392 \times 1040$  and the sensor chip dimension is  $2/3"$ . Dynamic range of the CCD sensor is 8-bit. Computer with 64 bit Intel (R) Core (TM) i5 microprocessor and CPU clock rate of 3.2 GHz was used to process the data. The digital hologram is stored in computer for further processing. In order to reconstruct the digital hologram, a digital reference wave  $R_D$  is used to reconstruct the digital transmitted wavefront  $O(m, n)$ , and is given by (Schnar and Juptner, 2005).

$$O = R_D H = R_D |R|^2 + R_D |O|^2 + R_D R^* O + R_D RO^* \quad (2)$$

At right hand side of equation (2), first two terms are dc term and correspond to the zero order diffraction and the third term is the twin image. The fourth term is the real image. To avoid the overlap between these three components (dc term, twin image and real image) during reconstruction, the

hologram is recorded in off-axis geometry. For this purpose, angle of reference beam ( $\theta$ ) with normal to CCD plane is adjusted such that  $\theta$  is sufficiently large enough to ensure separation between real and twin images in reconstruction plane. However, the angle  $\theta$  should not be small enough so that spatial frequency of micro interference pattern does not exceed than the resolving power of CCD sensor (Schnar and Juptner, 2005, p. R92).

## 2.1 Hologram Reconstruction

In digital holography reconstruction of object wavefront is done by numerical methods by simulating the diffraction of reference wave at the microstructure of recorded digital hologram using scalar diffraction theory. The most commonly used numerical reconstruction methods are Fresnel reconstruction method, convolution method, and phase shifting method. The diffraction of reconstructing wave at the digital hologram is described by the Fresnel-Kirchhoff integral (Schnar and Juptner, 2005, p. R90; Wagner et al., 1999). ( $X_O$ ,  $Y_O$ ), ( $X$ ,  $Y$ ), and ( $X_I$ ,  $Y_I$ ) are the Cartesian co-ordinate system of the object, hologram and image planes respectively (see Fig. 2).

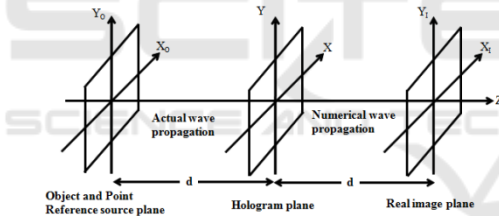


Figure 2: Cartesian co-ordinate system used in the Fresnel Reconstruction method.

The digital form of complex amplitude of diffracted wave in the reconstruction (image) plane using the Fresnel-Kirchoff diffraction integral with the Fresnel approximation is given by (Kumar et al., 2015, p. 1258)

$$O(m\Delta X_I, n\Delta Y_I) = \frac{i}{\lambda d} \exp[-i\pi\lambda d(\frac{m^2}{M^2\Delta X^2} + \frac{n^2}{N^2\Delta Y^2})] \times \text{FFT}\{R_D(p, q)H(p, q)\exp[-i\frac{\pi}{\lambda d}(p^2\Delta X^2 + q^2\Delta Y^2)]\} \quad (3)$$

where  $m$ ,  $n$  and  $p$ ,  $q$  are the integers ( $m, p = 0, 1, 2, 3, \dots, M-1$ ; and  $n, q = 0, 1, 2, 3, \dots, N-1$ ).  $M \times N$  are the number of pixels in the CCD sensor.  $\Delta X$  and  $\Delta Y$  are the pixel size of CCD sensor.  $H(p, q)$  is the recorded digital hologram,  $\lambda$  is the wavelength, and  $d$  is the reconstruction distance respectively.

If we assume that reference wave is a plane wave of wavelength  $\lambda$ ,  $R_D$  can be expressed as:

$$R_D = \exp\left[i\frac{2\pi}{\lambda}(k_x p\Delta x + k_y q\Delta y)\right] \quad (4)$$

Where  $k_x$  and  $k_y$  are the components of wave vector.

To remove the dc term and -1 order term, the recorded raw digital hologram  $H(p, q)$  is filtered in Fourier domain (Takeda et al., 1989; Cuche et al. 2000). For this purpose, first we perform the Fourier transform on  $H(p, q)$ , and the Fourier spectrum of  $H(p, q)$  gives the zero order term (dc term), +1 order and -1 order. Now to remove the dc term and -1 order term, rectangular band pass filter is applied on the +1 order term. The inverse Fourier transform of the selected spectrum (+1 order) provide the complex amplitude containing information about the object wavefront  $O(m\Delta X, n\Delta Y, Z=0)$ . Complex amplitude  $O(m\Delta X, n\Delta Y, d)$  at a distance  $d$  parallel to CCD plane is computed from the filtered spectrum by using equation (3).

Numerical reconstruction of recorded digital hologram  $H(p, q)$  yields the complex amplitude of object wavefront. Once the complex amplitude of object wavefront is calculated, the intensity and phase of the object can be calculated. The intensity of object wavefront is calculated as (Schnar and Juptner, 2005, p. R89)

$$I(m\Delta X_I, n\Delta Y_I) = |O(m\Delta X_I, n\Delta Y_I)|^2 \quad (5)$$

The phase is calculated as

$$\phi(m\Delta X_I, n\Delta Y_I) = \arctan \frac{\text{Im}[O(m\Delta X_I, n\Delta Y_I)]}{\text{Re}[O(m\Delta X_I, n\Delta Y_I)]} \quad (6)$$

where, the operators Re and Im denote real and imaginary part of a complex function.

The phase of the two states of object (initial and final) are evaluated individually from complex amplitude of object wave front in two states  $O_1(m\Delta X_I, n\Delta Y_I)$  and  $O_2(m\Delta X_I, n\Delta Y_I)$ .

Interferometric comparison i.e. phase difference provide information about change between two states. The phase of initial state and final states can be written as

$$\phi_1(m\Delta X_I, n\Delta Y_I) = \arctan \frac{\text{Im}[O_1(m\Delta X_I, n\Delta Y_I)]}{\text{Re}[O_1(m\Delta X_I, n\Delta Y_I)]} \quad (6a)$$

$$\phi_2(m\Delta X_I, n\Delta Y_I) = \arctan \frac{\text{Im}[O_2(m\Delta X_I, n\Delta Y_I)]}{\text{Re}[O_2(m\Delta X_I, n\Delta Y_I)]} \quad (6b)$$

The phase takes values between  $-\pi$  and  $\pi$ , the principal value of arctan function. The interference phase, which is phase difference between the phase in presence of object (micro-lens array) and absence of micro lens array, is calculated by modulo  $2\pi$  subtraction (Schnar and Juptner, 2002, p. R94)

$$\Delta\phi(m,n) = \begin{cases} \phi_2(m,n) - \phi_1(m,n) & \text{if } \phi_2(m,n) \geq \phi_1(m,n) \\ \phi_2(m,n) - \phi_1(m,n) + 2\pi & \text{if } \phi_2(m,n) < \phi_1(m,n) \end{cases} \quad (7)$$

The modulo  $2\pi$  phase difference map of micro-lenslet array and ambient air is unwrapped using Goldstein phase unwrapping method to remove the  $2\pi$  phase discontinuity (Goldstein, 1988).

### 3 EXPERIMENT RESULTS AND DISCUSSION

Initially the experiment was carried out on USAF resolution test chart. Figure 3(a) shows the recorded hologram of the USAF Resolution test target.

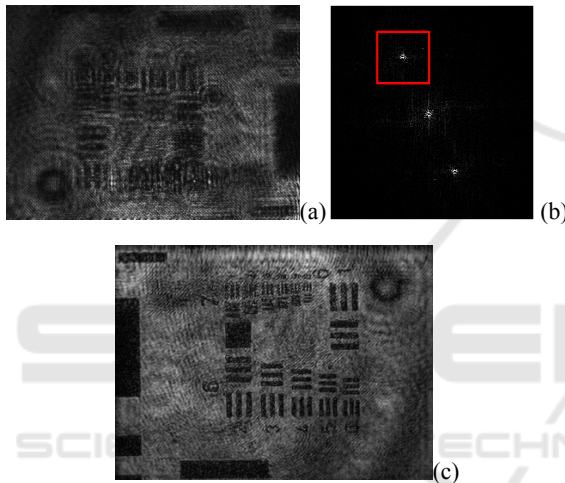


Figure 3: (a) Hologram of USAF resolution chart (b) Fourier spectrum of hologram (c) Intensity image.

A Fourier spectrum of the hologram gives the virtual image, real image and dc term (zero order diffraction). Figure 3 (b) shows the Fourier spectrum of the recorded digital hologram of USAF resolution test chart. A band pass rectangular filter is applied to remove the dc term and twin image. Inverse Fourier transform gives complex amplitude of object wavefront at CCD plane. Complex amplitude of object wavefront in reconstruction plane is calculated by solving equation (3). The intensity image of the USAF resolution test chart is evaluated using equation (5) and is shown in Figure 3(c). From the intensity image of resolution test target, it is clear that we are able to resolve the small details of 6<sup>th</sup> element of 7<sup>th</sup> group and it corresponds to 228.1 lines pair/mm (i.e width of one line is 2.19  $\mu\text{m}$  in USAF resolution test target). For resolving one line, the width of one line (2.19  $\mu\text{m}$ ) should be covered by at least two pixels. The achieved resolution

(1.095  $\mu\text{m}$ ) from the holographic set up agrees with the predicted resolution limit of the microscope objective (20X, NA=0.40). The resolution limit of microscope objective is given by Abbe criterion ( $0.61\lambda/\text{NA} = 0.965 \mu\text{m}$ ).

#### 3.1 Results of Testing of Micro-lens Array

First, we record a digital hologram of ambient air (in absence of micro-lens array) as a reference hologram. Now, micro-lenses array is mounted on 2D translational stage and inserted in the object arm of the Mach-Zehnder interferometer. In presence of micro-lenses array second digital hologram is recorded. Phases in the two individual states of object (ambient air and presence of micro-lenses array) are numerically reconstructed from equation (6a) and (6b) respectively. Fig.4 (a) shows the modulo  $2\pi$  phase difference map of micro-lenses and ambient air. The modulo  $2\pi$  phase difference map of micro-lenses and ambient air is unwrapped using Goldstein phase unwrapping method to remove the 2

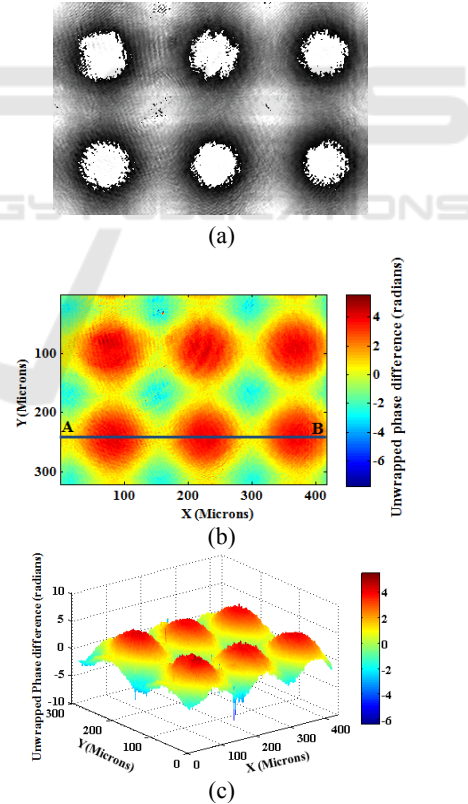


Figure 4: (a) Modulo  $2\pi$  phase difference, (b) 2D unwrapped phase difference map of Micro-lens array and ambient air, and (c) 3D unwrapped phase difference map of Micro-lens array and ambient air.

$\pi$  phase discontinuity. Fig. 4(b) shows the 2D unwrapped phase difference map of micro-lens and ambient air. Fig. 4(c) shows the 3D unwrapped phase difference map of micro-lenses and ambient air.

Now the optical path length difference ( $\Delta n \times h$ ) can be connected to experimentally calculated unwrapped phase difference through the equation

$$\Delta\phi = \frac{2\pi}{\lambda} \Delta n \times h \quad (8)$$

where  $\Delta n$  is the refractive index change ( $n-n_0$ ),  $n$  is refractive index of micro-lens material and  $n_0$  is the refractive index of ambient air, and  $h$  is the distance travelled by laser light ( $\lambda=632.8$  nm) through the micro-lens array.

Micro-lenses array is made up of fused silica. Consider, the refractive index of micro lenses array material is homogeneous. The refractive index of the fused silica is  $n = 1.457$  at wavelength 632.8 nm. Refractive index of air  $n_0=1$ . The height distribution of the micro-lenses can be evaluated from equation (8). Fig. 5(a) shows the 3D height map of the micro-lenses array. Fig. 5(b) shows the height profile of micro-lenses along the line AB as marked in Fig. 4(b).

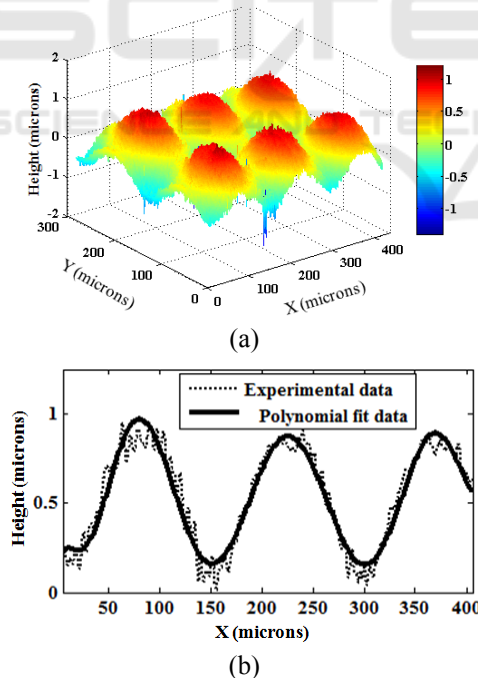


Figure 5: (a) 3D height map of micro-lens Array (b) Height profile of micro-lenses along the line AB as marked in Fig. 4(b).

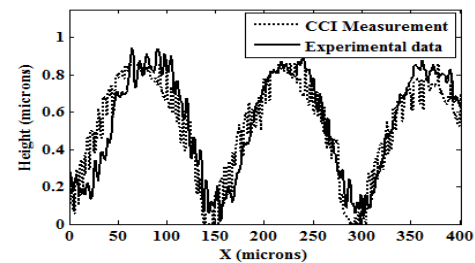


Figure 6: Comparison of height profiles of micro-lenses array obtained by digital holographic interferometric microscopy (DHIM) and Coherence Correlation Interferometer.

The diameter of micro-lens in the micro-lenses array is  $D=146$   $\mu\text{m}$  and experimentally evaluated maximal height (sag) of micro-lens of micro-lens array is  $h = 0.81$   $\mu\text{m}$ . From these values, the radius of curvature (ROC) is computed according to equation (Kühn et al., 2007).

$$ROC = \frac{h}{2} + \frac{D^2}{8h} \quad (9)$$

The computed value of radius of curvature of the micro-lens array is 3289.91  $\mu\text{m}$ . The sag height of micro-lens agrees well within the experimental limit as provided in the specification by the manufacturer (0.87  $\mu\text{m}$ ).

Height profile of micro-lenses measured by DHIM is compared with commercially available Coherence Correlation Interferometer (Manufacturer: Taylor Hobson Ltd. UK, Axial resolution 0.1  $\text{\AA}$ ). Fig.6 shows the comparison of height profiles of micro-lenses array obtained by DHIM and Coherence Correlation Interferometer (CCI). Root mean square error (RSME) between the measurement done by DHIM and CCI is 0.12 %.

## 4 CONCLUSIONS

In this paper Mach-Zehnder based off-axis digital holographic interferometric microscope (DHIM) is applied to test the micro-lens array. In the experiment, round shape and plano-convex micro lens array supplied by THORLABS with micro lens sag height ( $h=0.87$   $\mu\text{m}$ ) and radius of curvature ( $ROC=3.063$  mm) was used. The measured value of sag height ( $h=0.81$   $\mu\text{m}$ ) and radius of curvature ( $ROC=3.289$  mm) of micro-lens array by using DHIM and data supplied by manufacturer deviate by 0.6  $\mu\text{m}$  ( $h=6.89\%$ ) and  $ROC=7.4\%$  respectively.

## ACKNOWLEDGEMENTS

The financial assistance received from the Defence Research and Development Organization (DRDO), Ministry of Defence, Government of India, under the project entitled ‘Testing of micro optics using digital holographic interferometry’ is highly acknowledged.

## REFERENCES

- Sinzinger, S., and Jahns, J., (1999). *Micro-optics*. New York: Wiley.
- Anderson, R. H. (1997) Close-up imaging of documents and displays with lens arrays, *Applied Optics*, 18 (4), p. 477- 484.
- Cormick, F. B. Mc., Tooley, F. A. P. , Cloonan, T. J., Sasian, J. M., Hinton, H. S., Merserau, K. O., and Feldblum, A. Y. (1999) Optical interconnections using microlens arrays. *Optical and Quantum Electronics*. 24 (4). p. S465-S477.
- Hou, T., Zheng, C., Bai, S., Ma, Q., Bridges, D., Hu, A., and Duley, W. W. (2015) Fabrication, characterization, and applications of microlenses. *Applied Optics*. 54(24), p. 7366-7377.  
www.suss-microoptics.com
- Reichelt, S. and Zappe, H. (2005) Combined Twyman-Green and Mach-Zehnder interferometer for microlens testing. *Applied Optics*. 44(27), p. 5786-5792.
- Weible, K. J., Volkel, R., Eisner, M., Hoffmann, S., Scharf, T., and Herzig, H. P. (2004) Metrology of refractive microlens arrays in *Optical Micro- and Nanometrology in Manufacturing Technology*, Proc. SPIE. 5458, p. 43-51.
- Wahba, H. H., and Kreis, T. (2009) Characterization of graded index optical fibers by digital holographic interferometry. *Applied Optics*. 48 (8), p. 1573-1582.
- Zhang, T., and Yamaguchi, I. (1998) Three-dimensional microscopy with phase-shifting digital holography. *Optics Letter*. 23(15), p. 1221-1223.
- Charrière, F., Kühn, J., Colomb, T., Cuche, F. M., E., Emery, Y., Weible, K., Marquet, P., and Depeursinge, C., (2006) Characterization of microlenses by digital holographic microscopy. *Applied Optics*. 45(5), p. 829-835.
- Schnars, U., and Jüptner, W., (1994) Direct recording of holograms by a CCD target and numerical reconstruction. *Applied Optics*. 33(2), p. 179-181.
- Cuche, E., Marquet, P., and Depeursinge, C., (1999) Simultaneous amplitude and quantitative phase-contrast microscopy by numerical reconstruction of Fresnel off-axis holograms. *Applied optics*. 38(34), p. 6994-7001.
- Cuche, E., Bevilacqua, F. and Depeursinge, C., (1999) Digital holography for quantitative phase-contrast imaging. *Optics Letter*. 24(5), p. 291-293.
- Schnars, U., and Jueptner, W. (2005) *Digital Holography: Digital Hologram Recording, Numerical Reconstruction and Related Techniques*. Berlin, Germany: Springer-Verlag.
- Anand, A., Chhaniwal, V. K., and Javidi, B., (2011), Imaging embryonic stem cell dynamics using quantitative 3-d digital holographic microscopy. *IEEE Photonics Journal*. 3(3), p. 546-554.
- Schnars, U. and Juptner, W. P. O. (2002) Digital recording and numerical reconstruction of holograms. *Measurement Science and Technology*. 13, p. R85–R101.
- Wagner, C., Seebacher, S., Osten, W., and Juptner, W., (1999) Digital recording and numerical reconstruction of lensless Fourier holograms in optical metrology. *Applied Optics*, 38(22), p. 4812–4820.
- Kumar, V., and Shakher, C., (2015) Study of heat dissipation process from heat sink using lensless Fourier transform digital holographic interferometry, *Applied Optics*. 54 (6), p. 1257-1266.
- Takeda,M., (1989) Spatial-carrier fringe-pattern analysis and its applications to precision interferometry and profilometry : an overview. *Proc. SPIE*. 1121. p. 73-88.
- Cuche, E., Marquet, P., and Depeursinge, C., (2000) Spatial filtering for zero-order and twin-image elimination in digital off-axis holography. *Applied Optics*. 39(23), p. 4070-4075.
- Goldstein, R. M., Zebker, H. A., and Werner, C., (1988) Satellite radar interferometry: two-dimensional phase unwrapping. *Radio Science*. 23(4), p. 713–720.
- Kühn, J., Charrière, F., Colomb, T., Cuche, E., Emery, Y., and Depeursinge, C., (2007) Digital holographic microscopy for nanometric quality control of micro-optical components. *Proc. of SPIE*, 6475.